Identification of the elastic-plastic properties of CrN coating on elastic-plastic substrate by nanoindentation using finite element method-reverse algorithm

Yamen Ben Ammar, Khalil Aouadi, Corinne Nouveau, Aurélien Besnard, Alex Montagne

Identification of the elastic-plastic properties of CrN coating on elastic-plastic substrate by nanoindentation using finite element method-reverse algorithm

Y. Ben Ammar [a,*], Khalil Aouadi [b,c], Corinne Nouveau [d], Aurélien Besnard [d], Alex Montagne [e]

[a] Laboratoire de recherche LR18ES45 sis à l'institut préparatoire aux études d'Ingénieur de Nabeul, Université de Carthage, Campus Universitaire, 8000 Mrezga, Tunisia
[b] Applied Mechanics and Systems Research Laboratory (LR03ES06), Tunisia Polytechnic School, University of Carthage, BP 743, Rue El Khawarizmi, La Marsa 2078, Tunisia
[c] Moroccan Foundation for Advanced Science, Innovation and Research (MAScIR), Rue Mohammed El Jazouli, Rabat Design Center, 10100 Rabat, Morocco
[d] Arts et Metiers Institute of Technology, LABOMAP, HESAM Université, UBFC, F-71250 Cluny, France
[e] Arts et Metiers Institute of Technology, MSMP, 8, Rue Boulevard Louis XIV, Lille Cedex 59046, France

Keywords:
Instrumented-indentation testing
Film/substrate system
Substrate effect
Composite hardness modeling
Elasto-plastic properties
Inverse finite element material modelling

A B S T R A C T

This paper proposes an identification methodology based on nanoindentation analysis of coating/substrate system to extract the elastic-plastic properties of coating materials on elastic-plastic substrate when the indenter penetration depth is greater than the film thickness. In order to accurately predict the elastic-plastic properties of the coating materials, a trust-region reflective optimization algorithm is integrated with the finite element analysis, in cooperation with the Jönsson and Hogmark model. The proposed reverse analysis algorithm modifies a predicted load-displacement (P-h) curve by changing the elastic-plastic properties of the coating and the substrate until it fits the experimental nanoindentation (P-h) curve. Numerical and instrumental indentations tests were carried out on a CrN film/Martensitic stainless steel substrate system to verify the proposed reverse method, by which Young's modulus (E), yield stress (σ_y), and work hardening exponent of the film were obtained. A sensitivity analysis is conducted to study the effect of the elastic-plastic properties of the CrN film/substrate on the (P-h) curve. The results showed a high impact to the loading and unloading part of the (P-h) curve due to variations in (E) and (σ_y) of the steel substrate compared to those of the CrN coating.

1. Introduction

The main challenge in the coating applications is to create the exactly predefined mechanical properties that represent their actual performance. Difficulties in measuring the mechanical properties of thin films by classical methods have led to the use of the indentation method in nanoscale. Although nanoindentation technique has attracted considerable attention in recent decades, one of the main issues affecting the measurement of properties of the thin film by this technique is the substrate effect [1-6].Generally, to prevent this problem, a common practice is to consider that the modulus of the thin film is not affected by the substrate for indentation depths smaller than 1/10 of the film thickness [7]. Then, Young's modulus (E) and hardness (H) of the film can be obtained through Oliver & Pharr method [8]. Nevertheless, this assumption rule is not valid for all the film/substrate systems because if the tested sample exhibits a pile-up rather than a sink-in phenomenon at the edge of residual indentation, the accurate contact depth will be underestimated and thus the calculated (E) and (H) will be overestimated [9]. Furthermore, a rough surface of the same order of magnitude as contact depth might induce errors at such a small scale. Studies have shown that the indentation experiments do not accord well with the indentation theory at a shallow depth, which is caused by the so-called indentation size effect (ISE).

An alternative approach to circumvent the above issues is to carry out indentation tests on a film/substrate system at a deep depth. Based on the analytical approach, many studies presented methods to evaluate Young's modulus of a thin film deposited on a substrate from an experimental nanoindentation test [10–12].The above models expressed Young's modulus of the composite as a function of Young's modulus of the film and the substrate. Other studies proposed mix law models to evaluate the composite hardness of coating/substrate systems such as Bückle [13], Jöhnson and Hogmark [14], Puchi-Cabrera [15],

* Corresponding author.
E-mail address: yamen_benammar@yahoo.fr (Y. Ben Ammar).

https://doi.org/10.1016/j.tsf.2022.139356

Korsunsky et al. [16] and Rahmoun et al. [17].

However, these analytical models do not provide plasticity characteristics of the coating from indentation experiments. The most suitable tool for this is the Finite Element Method (FEM), which has been widely applied to indentation testing with the objective of obtaining information about the plastic properties of the coating [18–20]. In this case, numerous other studies proposed mechanical characterization models for the coated systems based on both the Dimensional Analysis Method (DAM) and the FEM [1,5,21-25].

As mentioned above, all these models can be distinguished according to two different criteria: Models based on DAM and FEM. However, most of these methods neglect the film thickness and the effect of elastic-plastic properties of the substrate which can affect the coating properties [25].

The aim of this study is the development of a methodology based on FEM-reverse analysis, in cooperation with the Jönsson and Hogmark (JH) model to accurately extract the elastic-plastic properties of the coating. The (JH) model is used to estimate Young's modulus and the yield stress (σ_y) of the coating and the substrate which will be integrated subsequently into the reverse analysis as input data. This study provides a simple methodology to accurately extract the elastic-plastic properties of the film by considering the influence of the elastic-plastic substrate from one indentation test. The uniqueness issue of the reverse analysis results is addressed by narrowing the range of the initial values of the material properties based on the literature data and the results given by the (JH) model.

The proposed method was then applied to a CrN film/steel substrate system deposited at different substrate bias voltages. The objective is to extract Young's modulus, yield stress, and the work-hardening exponent (n) of the CrN coating in each case and to evaluate the effect of the substrate bias voltage on the mechanical properties of the coating.

2. Materials and methods

2.1. Materials and samples preparation

2.1.1. Substrates

Chromium nitride (CrN) films were deposited on stainless steel (90CrMoV8) samples (20 × 20 mm^2 and 5 mm thick) with a surface roughness Ra of 0.5 μm and on mirror-polished silicon (100) samples (10 × 10 mm^2 and 380 μm thick). Before deposition, all the substrates were ultrasonically cleaned in acetone and ethanol for 5 min each and then dried under compressed air.

2.1.2. Coatings

The CrN coatings were deposited by Direct Current (DC) reactive magnetron sputtering (KENOSISTEC-KS40V). Before deposition, all substrates were in situ etched under argon plasma at −700 V for 10 min to ensure a better adhesion of the coatings. The substrate temperature during applying substrate bias voltage of −700 V is about 300 °C which is below the tempering of the steel substrate. Prior to deposition, the residual pressure was lower than 2 × 10^{-5} Pa and the chamber was heated at 300 °C for 7 h. During deposition, the working pressure was set at 0.5 Pa. The flow rates of Ar and N_2 were 68.8 and 33.3 sccm, respectively. A chromium target with apurity of 99.95% and (406.4 × 127) mm^2 dimensions wasused for the deposition process. The Chrominum (Cr) target power was set at 1500 W (−375 V). We applied a substrate bias voltage of −200, −500 and −700 V to study its effect on the mechanical properties of the CrN films. The deposition time was fixed to 2 h. Table 1 summarizes the CrN deposition conditions.The microstructures of the obtained coatings were observed by Scanning Electron Microscope (SEM) field emission (JEOL JSM7610F). The operational voltage was kept at 15 kV and its minimum spot size was approximately 1 μm. Fig. 1 shows the microstructure of the CrN films as a function of the substrate bias voltage. The SEM images showed that CrN coatings present a columnar and dense microstructure when increasing the substrate bias voltage. The film's thicknesses vary between 0.87 to 1.14 μm.

Table 1
Deposition conditions of the CrN coatings.

Argon flow rate (sccm)	68.8
Nitrogen flow rate (sccm)	33.3
Working pressure (Pa)	0.5
Deposition time (h)	2
Temperature (°C)	300
Substrate bias voltage (V)	−200, −500, −700
Power of the Cr target (W)	1500
Target bias voltage (V)	−375

2.2. Nanoindentation tests

The hardness of CrN coatings has been measured by means of nanoindentation tests using an XP instrument (MTS, USA) equipped with a Berkovich diamond tip. The maximum load is about 750 mN and the indentation depth varies between 1.9 and 2.1 μm. A minimum of nine indents has been performed on each sample. The nanoindenter worked in strain-rate controlled mode, set at the constant value of 0.05 s^{-1}.To allow a continuous characterization of (H) and (E) of the coating during the indentation process, tests were performed using the CSM (Continuous Stiffness Measurement) mode [26]. To observe the influence of the substrate, the indenter reached a penetration depth higher than the thickness of the coatings. Neighboring indents were spaced by 35 times the maximal penetration depth, to avoid interactions. In this case, due to the large indentation depths, the mechanical properties depend on the coating and on the substrate effect. In order to take in to account the substrate effect on the determination of the mechanical properties of the film, it is necessary to determine the film and substrate hardness i.e. Young's modulus separately from the measured composite hardness i.e. composite modulus. That is why we used the (JH) model. Fig. 2 shows the experimental load-displacement (P-h) curves for the three applied substrate bias voltages (−200, −500 and −700 V).

2.3. Mathematical modeling

The (JH) model was used to calculate (H) and (E) of the film when the indenter penetration is influenced by the substrate. In this model, the composite hardness of the coating system is related to the hardness of the coating and the substrate by a mixture law. Hence, the volume fraction of the coating material, which contributes to the composite hardness, a_f, expressed in terms of indentation depth, h, is given by the Eq. (1):

$$a_f = 2\frac{C\,t_f}{h} - \frac{C^2\,{t_f}^2}{h^2} = 1 - \left(1 - \frac{C\,t_f}{h}\right)^2 \quad (1)$$

where C is a constant, which depends on the indentation behavior ofthe coating material and indenter geometry [17] and t_f is the coating thickness. If under indentation loading employing a Berkovich indenter the coating undergoes fracture, C = 0.0915, whereas if the coating undergoes plastic deformation, C = 0.1746. Since the volume fraction of the coating material should fulfill the condition that $0 < a_f < 1$, Eq. (1) is ill-defined, since if $h < C.t_f$, a_f does not tend to 1, as it should. Thus, the above definition should be complemented by Eq. (2):

$$\begin{cases} a_f = 1 & if\ h < C\,t_f \\ a_f = 1 - \left(1 - \dfrac{C\,t_f}{h}\right)^2 & Otherwise \end{cases} \quad (2)$$

Thus, for a monolayer coating the composite hardness, Hc, would be given by Eq. (3):

$$H_c = a_f H_f + (1 - a_f) H_s \quad (3)$$

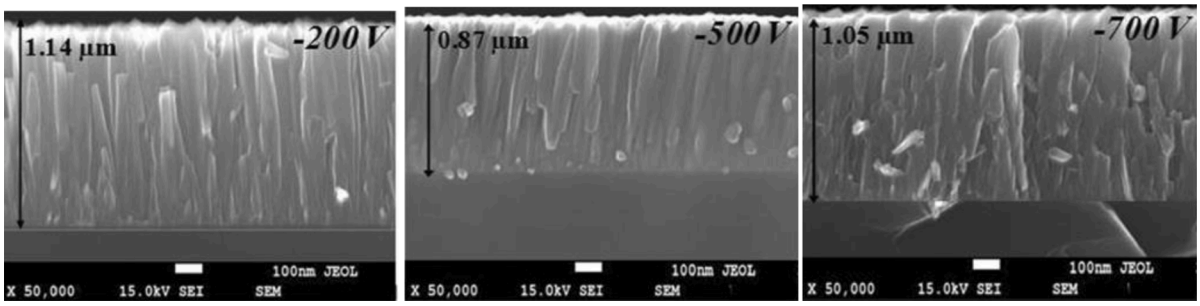

Fig. 1. .Cross-sectional SEM images of the CrN coatings as a function of the substrate bias voltage.

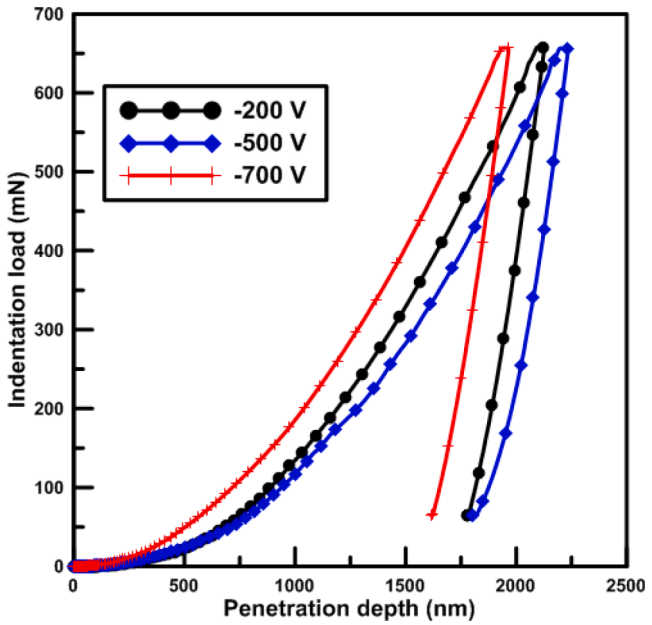

Fig. 2. .Experimental (P-h) curves corresponding to −200 V,−500 V and −700 V substrate bias voltages.

where H_f represents the intrinsic hardness of the coating and H_s is the substrate hardness. Thus, given the ill-definition of a_f, from the computational viewpoint, to determine simultaneously the values of both H_f and H_s, the composite hardness should be defined as follows:

$$\begin{cases} H_c = H_f & if\ h < C\ t_f \\ H_c = a_f H_f + (1 - a_f) H_s & Otherwise \end{cases} \quad (4)$$

In this model, the mechanical properties of the coating and substrate are considered independent of the penetration depth. However, the weight function, a_f, for the composite hardness (Eq. (3)) is, indeed, dependent of the penetration depth (Eq. (2)). Hence, the proposed model gives a unique value of (H) for coating and susbtrate. Furthermore, additional problem often occurs when studying hardness evolution, i.e. the indentation size effect which traduces the load-dependence of the nano and micro-hardness. The nanohardness is generally higher than the micro or macrohardnesses due to the indentation size effect. In this work, the (JH) model was improved by incorporating the (ISE) effect taking into account a linear relation between hardness and the reciprocal indentation depth. The description of the experimental hardness data by means of this model gives the absolute hardness i.e. the macrohardness independent of the applied load for coating (H_{f0}) and susbtrate (H_{S0}), by assuming that [17]:

$$H_f = H_{f0} + \frac{B_f}{h} \quad and \quad H_s = H_{s0} + \frac{B_s}{h} \quad (5)$$

where Hf0 and Hs0 represent the intrinsic hardness (disregarding any ISE) of the layer and substrate, respectively, whereas Bf and Bs are the corresponding (ISE) parameters.

Therefore, equations (4) through (5) encompass the computational procedure that should be followed to determine the change in the composite hardness with penetration depth for a monolayer coating, according to the model advanced by Iost et al. [17]. Also, by means of non-linear least square analysis, it allows the computation of the intrinsic hardness of the layers, as well as that of the substrate.

The same model was used to determine Young's modulus of the coating and of the substrate, considering C as a variable depending on the material [2,27]. This constant was lower than the value used for the determination of the hardness since the elastic zone extended further than the plastic zone.

Thus, for a monolayer coating the composite modulus, Ec, would be given by Eq. (6:)

$$E_c = a_f E_f + (1 - a_f) E_s \quad (6)$$

where, E_f represents Young's modulus of coating, E_s represents Young's modulus of substrate and a_f represents the volume fraction expressed by Eq. (1). In order to determine simultaneously the values of (E_f) and (E_s), the composite modulus (E_c) should be defined as follows:

$$\begin{cases} E_c = E_f & if\ h < C\ t_f \\ E_c = a_f E_f + (1 - a_f) E_s & Otherwise \end{cases} \quad (7)$$

2.4. Finite element modeling

2.4.1. Axisymmetric FEM models

In this study, the indentation test of the system, using a Berkovich indenter, has been numerically simulated using the Abaqus Standart 2017 FE code. The coating/substrate couple was modeled using over 8123 four-node axisymmetric elements with reduced integration (CAX4R), where the mesh was designed gradually coarse away from the contact region of indenter/specimen to the distal end. To simulate the semi-infinite substrate, the coating/substrate system dimension was fixed to 25 × 70 µm^2 with a film thickness of 1 µm (Fig. 3). For the Berkovich indenter, an axisymmetric deformable body with reduced integration (CAX4R) is used. The region of interest is in the vicinity of the perfect (sharp) indenter tip where a high element density with finer mesh size (0.2 and 0.3 µm) has been used due to the expected high stress gradients immediately beneath the indenter tip, as shown in Fig. 3.A full adhesion between the film and the substrate was required by assuming that the film and the substrate are perfectly bonded and there is no delaminating or slippage at the interface.The friction coefficients at the contact surfaces between the indenter and the top surface of the CrN thin layer are assumed tobe zero since friction has a negligible effect on the indentation process [1]. A "master-slave" contact scheme in the FE procedure is applied on the indenter and the specimen surface. All nodes at the base of the specimen are constrained to prevent them from moving in the x and y directions. A deformable conical indenter with a 70.3° face

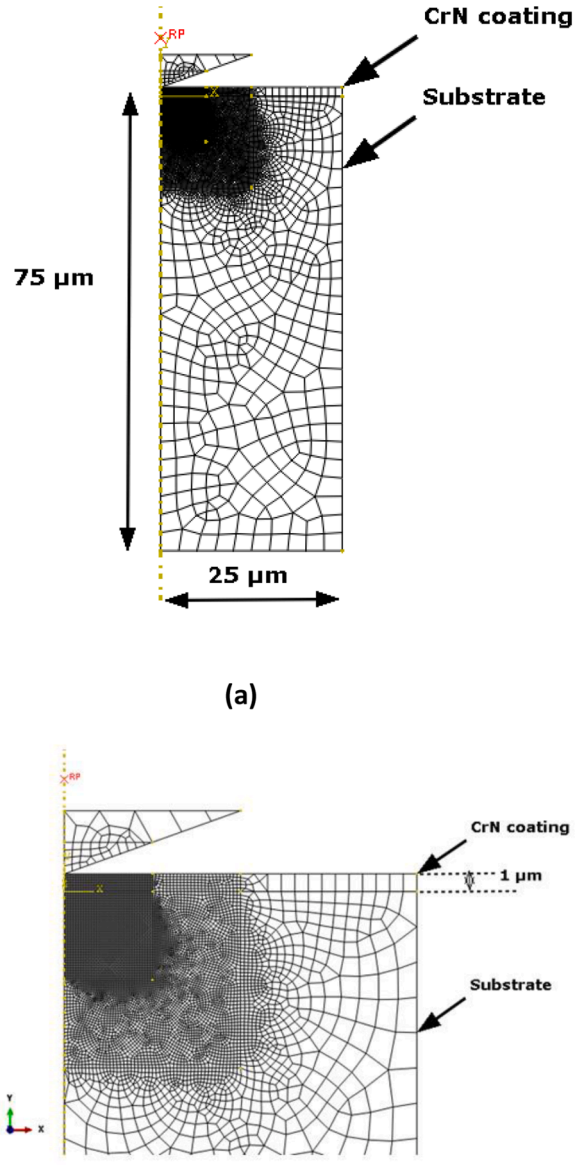

Fig. 3. (a) FEM model with adaptive meshing resulting in 8123 elements. (b) Magnified view of a dense mesh area close to the indenter contact.

angle is used, which gives the same projected area to depth-ratio as a Berkovich and Vickers indenters. This way the real and more complex 3D Berkovich model is reduced to an axisymmetric one allowing to solve numerically a 2D problem and thus simplifying the numerical analysis and accelerating the process of nanoindentation reverse analysis procedure. Generally, the relationships between the applied indenter displacement (h) and the reaction force (P) with axisymmetric and Berkovitch 3D models are in good agreement [28].

The simulations are carried out in two distinct steps: a loading step and an unloading step. In the first step, the total indenter displacement is imposed. During the loading step, the deformable indenter moves downwards along the axial-direction to penetrate the substrate up to the maximum specified depth. During the unloading step, the indenter is unloaded and returns to its initial position. The proposed FE simulations do not model the indentation size effects and are therefore limited to simulating macro indentations.

2.4.2. *Elastic plastic material constitutive model*

In this study, the diamond Berkovich indenter was assumed linear elastic and perfectly plastic material with 1024 GPa for Young's modulus, 0.07 for Poisson ratio and 35.7 GPa for yield stress [19]. A power law strain hardening curve has been used for the CrN coating and the steel substrate to simulate the indentation experiments.In this case, the stress-strain (σ-ε) relationship is assumed to be:

$$\sigma = \begin{cases} E\varepsilon \quad for \quad \varepsilon \leq \dfrac{\sigma_y}{E} \\ K\varepsilon^n \ for \quad \varepsilon > \dfrac{\sigma_y}{E} \end{cases} \tag{8}$$

where σ represents the true stress, ε represents the total strain, E is the Young's modulus, n is the strain hardening coefficient and σ_y is the yield stress.

The decomposition of the strain into elastic and plastic parts is given by Eq. (9):

$$\varepsilon_{total} = \varepsilon_{el} + \varepsilon_{pl} \tag{9}$$

Since all plastic strains should be input as true strains in ABAQUS, the stress equation can be written as:

$$\sigma = K\left(\frac{\sigma_y}{E} + \varepsilon_{pl}\right)^n \tag{10}$$

where K is given by Eq. (11):

$$K = E^n \sigma_y^{1-n} \tag{11}$$

In the ABAQUS input file, a discrete set of points is required to represent the uniaxial stress-strain data, rather than specifying the work-hardening exponent (n). To specify the plastic stress-strain data in ABAQUS, the coefficient K can be calculated by using Eq. (11) and the updated stress data related to each plastic strain value can be obtained by Eq. (10).

2.5. *Optimization analysis*

In this work, a non-linear optimization technique is devised within the MATLAB R-2019a optimization toolbox [29] which provides an excellent interface to FE codes such as ABAQUS. To perform connection between the finite element modeling ABAQUS and the mathematical analysis MATLAB, a software tool named Abaqus2Matlab [30] is proposed. It allows to run ABAQUS directly from MATLAB and to post-process the results, providing a link between the two well-known packages. Thus, the optimization procedure is used to determine mechanical properties for a given set of experimental indentation data using an iterative procedure based on a MATLAB nonlinear least-squares routine to produce the best fit between the given experimental indentation data and the optimized indentation data, produced by the proposed methods. This non-linear least-squares optimization function (called LSQNONLIN) is based on the trust-region reflective algorithm [29]. This approach was used to solve bound-constrained nonlinear minimization problems. In order to describe this approach, assuming F (x) is an objective function to be minimized with x as a vector. The vector x has a nonlinear relationship with the material response, which makes the problem become multivariable nonlinear. To solve this kind of problem, the trust-region approach is the most suitable one because of its boundedness. Furthermore, trust-region algorithms are reliable and robust and they have very strong convergence properties. The value of x can be bounded by upper bound (ub) and lower bound (lb) constrains (i.e. lb $\leq x \leq$ub). In this approach, the optimum values of the parameters can be ensured by several termination tolerances and the number of iterations in the optimization process. The termination tolerances include the minimum changes in the values of the variables (i.e. the model parameters) and the minimum changes in the value of the objective function F(x). In this study, the adopted tolerances for both

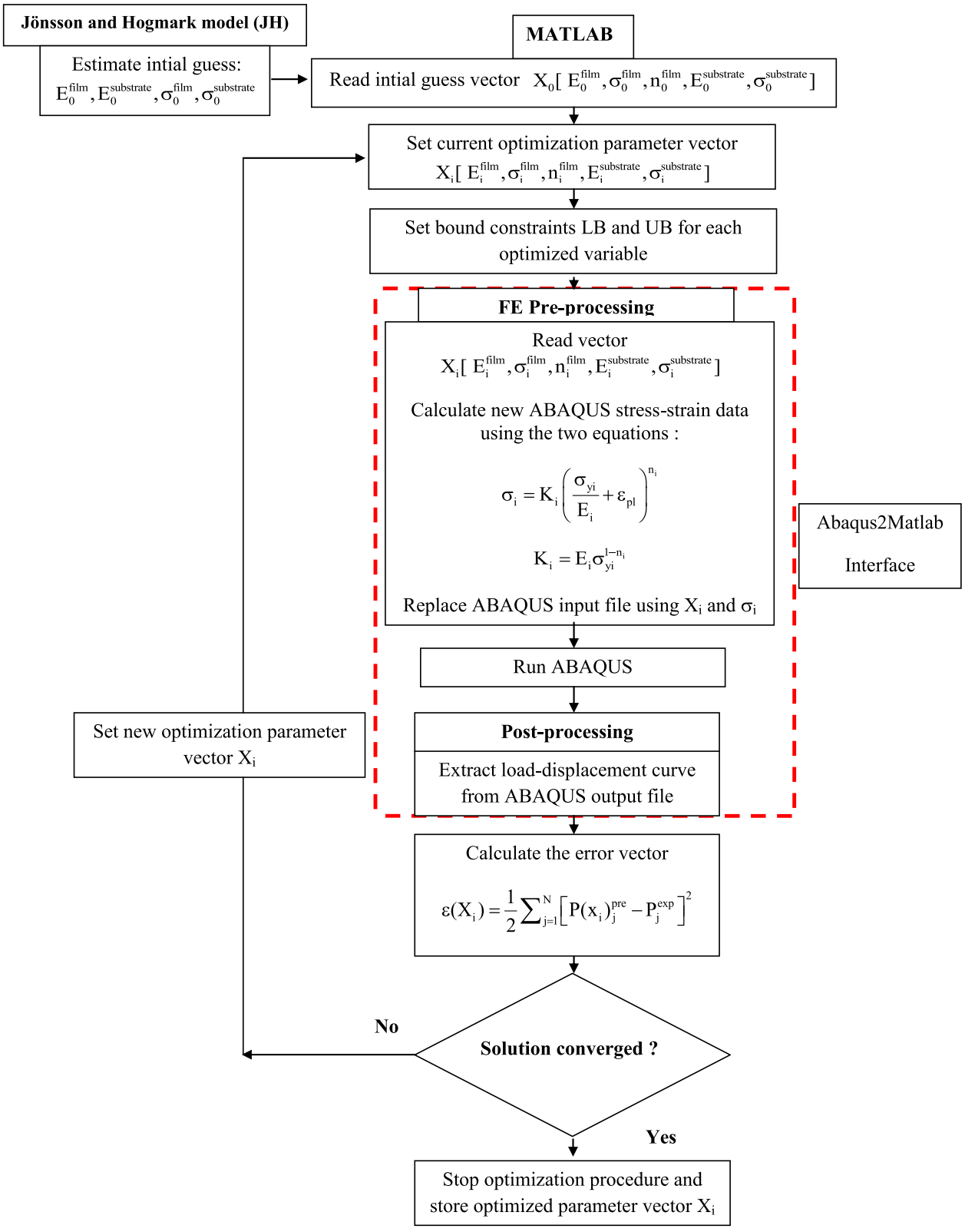

Fig. 4. Flowchart of the optimization algorithm to determine the mechanical properties of the coating/substrate system.

variables and functions were 10^{-2} to ensure the accuracy of the optimized model parameters. Applying the trust-region reflective algorithm, the upper and lower bound constraints for the variables (i.e. the elastic-plastic properties of coating and substrate) can be set to avoid the impractical values and to ensure the accuracy of results.

The MATLAB code was then used to automatically run the ABAQUS input file to iteratively determine the error between experimental and optimized load-displacement curves. The goal is to reduce the sum of the squared error in the prediction of indentation depth at each load increment point (i) until convergenceis reached. The error criterion is

based on the use of objective function until a minimum convergence value within the range of 10^{-2} is achieved. The objective function is defined by Eq. (12):

$$F(x) = \frac{1}{2}\sum_{i=1}^{N}\left[P(x)_i^{pre} - P_i^{\exp}\right]^2 \rightarrow \min \tag{12}$$

$$x \in R^n$$

$$LB \leq x \leq UB$$

where F(x) represents the objective function, x represents the optimization variable set which for this specific case contains the full set of the material constants in the model $x = [material\,properties\ (E, \nu, \sigma_y, n, ...)]^T$, LB and UB represent the lower and upper boundaries constraints of x allowed during the optimization in order to address the non-uniqueness issue of the inverse analysis of indentation purely based on experimentally and finite element simulated (P-h) curves [28,31,32], $P(x)_i^{pre}$ and $P_i^{\exp}$ represent the predicted total force and the experimental force from target data, respectively, at specific position i, within the loops. N is the total number of points used in the measured load-displacement loop.

In order to ensure the accuracy of the results, the estimated values of material properties measured by the (JH) model have been chosen as

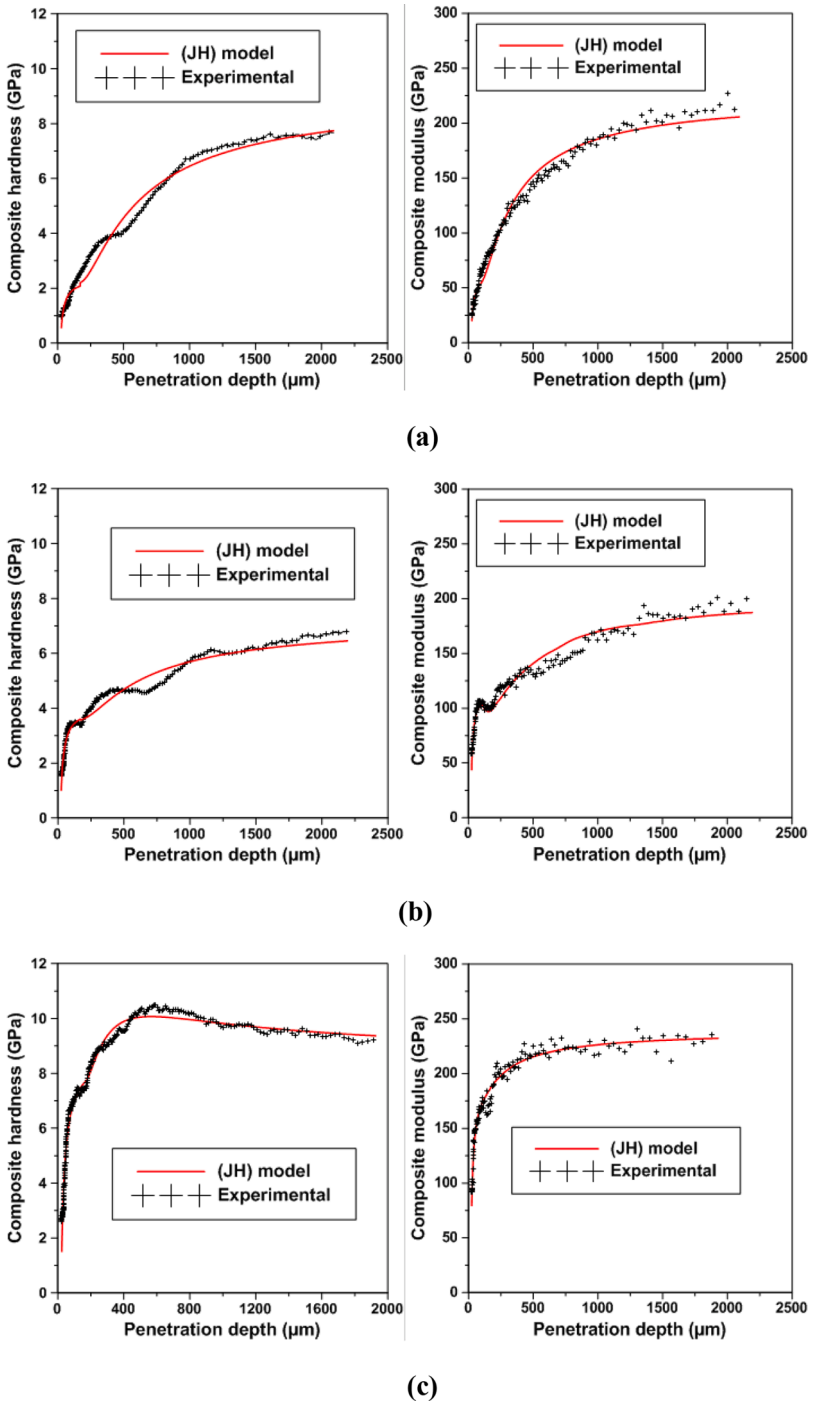

Fig. 5. Composite hardness and composite modulus as a function of the penetration depth for the three nanoindentation tests: (a)−200 V, (b) −500 V, and (c) −700 V. The solid line corresponds to the interpretation of the experimental results by the (JH) model.

initial values in the optimization process and the proposed trust-region algorithm has been used to find the optimized values of material parameters from which the best fit between the experimental and predicted loading-unloading curve can be achieved. The schematic diagram of the optimization approach is shown in Fig. 4.

3. Results and discussion

3.1. (JH) model results

Fig. 5 illustrates the change in the composite hardness and composite modulus as a function of the penetration depth as determined from the three nanoindentation tests (−200 V, −500 V, and −700 V). As can be seen in Fig. 5(a), for a substrate bias voltage of −200 V, the composite hardness and composite modulus increase with the penetration depth and tend to stabilize at large penetration depths. We note here that this behavior is like that observed for ductile coatings deposited on hard substrates [17,33]. The same trend is observed for a substrate bias voltage of −500 V (Fig. 5(b)). Furthermore, the subsequent increase in composite hardness and composite modulus with the penetration depth indicates that the steel substrate should exhibit higher intrinsic hardness and Young's modulus than those of CrN coating as should be confirmed from the modeling results. Contrariwise, for a substrate bias voltage of −700 V, see Fig. 5(c), the composite hardness and composite modulus tend to increase with the penetration depth and reach a maximum of 10.5 GPa for the composite hardness at approximately 650 nm of penetration depth, and of 230 GPa for composite modulus at approximately 400 nm of penetration depth. Thereafter, the composite hardness and composite modulus decrease and tend to stabilize at large penetration depths. Therefore, it is expected that the decrease in hardness from a penetration depth which represents approximately 50% of the CrN coating thickness, is related to the high hardness of the CrN coating compared with that of the steel substrate. For Young's modulus, it seems that its values for coating and steel are close.

To describe the experimental data by means of the (JH) model, we consider, for the determination of intrinsic hardness that the CrN coating tends to deform plastically. Therefore, by setting C(CrN) = 0.1746, a non-linear least-squares optimization function called « fminsearch » is programmed in MATLAB to determine the intrinsic hardness of the CrN coating, as well as that of the steel substrate by fitting the experimental data (see Fig. 5). The same procedure is used to determine their Young's modulus in which the constant C is also optimized (see Eqs. (1) and (7)). Fig. 5 illustrates the final description of the experimental hardness and Young's modulus data by means of this model and Table 2 summarizes the values of the different parameters involved in the model.

As can be observed in Fig. 5, the (JH) model is able to provide a satisfactory description of the change in the composite hardness and composite modulus of the coated system as a function of the penetration depth. Accordingly, the model predicts that up to a penetration depth of approximately 175 nm, the composite hardness will increase, and its value will be determined by the intrinsic hardness of CrN coating, respectively 3.42 GPa for −200 V, 4.2 GPa for −500 V, and 9.9 GPa for −700 V. The same trend is observed in the case of the composite modulus, but up to a penetration depth of approximately 10% of the film thickness, with 67 GPa for −200 V, 121 GPa for −500 V, and 211 GPa for −700 V. As the penetration depth increases the steel substrate starts to contribute to the composite hardness and composite modulus in two ways. For substrate bias voltages of −200 V and −500 V, an increase in the composite hardness and composite modulus is observed, and at large penetration depth, these two variables tend to stabilize. Otherwise, for substrate bias voltage of −700 V, the composite hardness and composite modulus increase up to a penetration depth of 650 nm and 400 nm, respectively. Thus, from these penetration depths, the steel substrate will start to contribute to its value, giving rise to a decrease in hardness and Young's modulus, as shown by the predicted curve in Fig. 5(c). This behavior is like that observed for hard coatings deposited on soft substrates [34]. In addition, at large penetration depth, the model predicted values of (H) and (E) will be determined by the intrinsic hardness and Young's modulus of the steel substrate.

These results prove that when the substrate bias voltage increases from −200 to −700 V, the hardness and Young's modulus of CrN coating increase too. These results have been proved by many authors [35,36]. This is probably due to the grain size effect [37]. In fact, when the grain size is small, the density is high and the effect of dislocation blocking increases [38]. Likewise, the structure densification process can improve hardness [39]. When the microstructure becomes denser, defects in coatings are effectively reduced.

Table 3 gives a literature oreview on the mechanical properties of CrN coating. The relatively low hardness and Young's modulus values that have been found for the CrN film coating in the present study compared with other works (Table 3) could be due to different reasons. It is well known that the hardness and Young's modulus of CrN films depend significantly on the deposition technique and also on the deposition conditions [48,50]. Another factor to take into account is the method used to measure these properties through the nanoindentation or microhardness tests. Indeed, the majority of works neglect the substrate effect in the calculation of the hardness and Young's modulus of the CrN coating in which the Oliver-Pharr method is usually used. Furthermore, the nanohardness is generally higher than the micro or macrohardnesses because of the indentation size effect. Thus, the calculated (E) and (H) are generally overestimated.

3.2. Simulation results

Three CrN coating/steel substrate systems deposited at −200 V, −500 V and, −700 V substrate bias voltages have been characterized using the inverse analysis technique proposed in this study. For these three analyses, the hypotheses of homogeneous and isotropic material were assumed.

3.2.1. Determination of elastic-plastic properties of the CrN coating

The assessment of the capability of this method to determine the elastic-plastic properties of each of the coating and the substrate choosing a set of initial guess material properties is summarized in Table 4.

In this work, a non-linear optimization approach, in cooperation with the (JH) model, is used to extract five elastic-plastic parameters of the coating/substrate system, using results from a single indentation curve. The elastic-plastic parameters to be extracted through the optimization are the young's modulus, yield stress and work hardening exponent of CrN coating, and Young's modulus and the yield stress of the steel substrate. However, obtaining a unique set of material

Table 2
Parameters involved in the (JH) model.

	Substrate bias voltage−200V		Substrate bias voltage−500V		Substrate bias voltage−700V	
	CrN coating	Substrate	CrN coating	Substrate	CrN coating	Substrate
H (GPa)	3.42	7.74	4.2	7.21	9.89	8.12
C.tf (nm)	0.1746 × 1000 (174.6)		0.1746 × 1000 (174.6)		0.1746 × 1000 (174.6)	
E (GPa)	67	221	121	205	211	225
C.tf (nm)	0.089 × 1000 (89)		0.071 × 1000 (71)		0.105 × 1000 (105)	

Table 3
Literature data on the mechanical properties of CrN coating.

	Values	thickness (μm)	Deposition technique	Substrate	Model
H (GPa)	26 [40]	0.8	DC–PVD*	stainless steel	Olivar and Phar (nanoindentation tests)
	24 [41]	2	DC–PVD**	cemented carbide	
	19 [42]	1.3	RF–PVD[2]	silicon	
	16 [43]	1	DC–PVD	silicon	
	13 [44]	0.3	RF–PVD	metallic glass	
	12 [45]	0.6	DC–PVD	silicon	
	10 [46]	0.3	RF–PVD	metallic glass	
	8.5 [47]	2	DC–PVD	stainless steel	Microhardness test
	5 [47]	2	DC–PVD	stainless steel	
	3–22 [48]	4–5	DC-PVD	stainless steel	
E (GPa)	437 [41]	2	DC-PVD	cemented carbide	Olivar and Phar (nanoindentation tests)
	360 [40]	0.8	DC-PVD	stainless steel	
	235 [45]	0.6	DC-PVD	silicon	
	170 [43]	1	DC-PVD	silicon	
	160 [44]	0.3	RF-PVD	metallic glass	
	100 [46]	0.3	RF-PVD	metallic glass	
	185 [49]	1	DC-PVD	silicon	Finite element analysis
σ_y (GPa)	12.78 [49]	1	DC-PVD	silicon	Finite element analysis
	4 [44]	0.3	RF-PVD	metallic glass	
	2.3 [41]	2	DC-PVD	cemented carbide	

* DC-PVD: direct current (DC) plasma assisted PVD.
** RF-PVD: radio-frequency (RF) plasma assisted PVD.

Table 4
Set up and results for optimization.

Substrate bias voltage (V)	Materials	Optimization parameter	Initial guess parameter	Bound constraints	Optimized parameters	Iteration
−200	CrN coating	(E)	67 [GPa]	$50<E[GPa]<240$	62.5 [GPa]	46
		(σ_y)	2 [GPa]	$1<\sigma_y[GPa]<14$	1.9 [GPa]	
		(n)	0.2	$0<n<0.5$	0.14	
	Steel substrate	(E)	221 [GPa]	$190<E[GPa]<240$	225 [GPa]	
		(σ_y)	2.2 [GPa]	$2<\sigma_y[GPa]<2.7$	2.31 [GPa]	
−500	CrN coating	(E)	121 [GPa]	$50<E[GPa]<240$	102 [GPa]	27
		(σ_y)	2 [GPa]	$1<\sigma_y[GPa]<14$	1.7 [GPa]	
		(n)	0.2	$0<n<0.5$	0.05	
	Steel substrate	(E)	205 [GPa]	$190<E[GPa]<240$	194 [GPa]	
		(σ_y)	2.2 [GPa]	$2<\sigma_y[GPa]<2.7$	2.05 [GPa]	
−700	CrN coating	(E)	211 [GPa]	$50<E[GPa]<240$	205 [GPa]	23
		(σ_y)	4 [GPa]	$1<\sigma_y[GPa]<14$	4.5 [GPa]	
		(n)	0.2	$0<n<0.5$	0.35	
	Steel substrate	(E)	225 [GPa]	$190<E[GPa]<240$	236 [GPa]	
		(σ_y)	2.2 [GPa]	$2<\sigma_y[GPa]<2.7$	2.43 [GPa]	

properties from a single indentation test has proved to be difficult, namely the uniqueness issue. Consequently, some researchers [28] used (P-h) curves obtained from more than one indenter geometry in order to obtain a unique set of material constants. In this study, the uniqueness issue can be addressed by narrowing the range of the guess values of the material properties. It is noted that convergence is faster, and with improved accuracy, when the initial guess values are chosen closer to the target values [28]. Moreover, it is reported that there are good agreements between the target and optimized values based on using a conical indenter, although the convergence rate and accuracy depend on the initial input values [28]. Iracheta et al. [51] reported that the non-uniqueness issue of the inverse analysis of indentation purely based on experimentally and FE simulated (P-h) curves, can be addressed by using a set of bound constraints (the lower and upper boundaries of variable x_i) in order to limit the space of possible solutions of x_i.

In this study, the (JH) model is used to estimate Young's modulus and the macroscopic hardness of both the coating and the steel substrate. The estimated values of Young's modulus (see Table 2) have been chosen as initial values in the proposed optimization algorithm (see Table 4). Moreover, the estimated values of macroscopic hardness were used to estimate the yield stress of both the coating and the substrate through the Tabor assumption derived for metals [52], H/c, where c is a constant which is normally taken as 3 for ideal plastic materials (i.e. those without work hardening behavior) undergoing sharp indentation [53]. Hence, the initial values of yield stress in the proposed optimization algorithm for the coating and the substrate have been chosen closer to the estimated values (see Table 4). Only the initial value of the work-hardening exponent of the coating was chosen arbitrarily, between 0.0 and 0.5.

Furthermore, in order to limit the space of possible solution and to ensure the accuracy of the estimation of the mechanical properties, the lower and upper boundaries of each variable are adjusted based on the literature data (see Table 3). For the steel substrate, the bound constraints have been defined as follows: for most steels, Young's modulus has a value between 190 and 225 GPa [51,54]. Although, based on (JH) model results, Young's modulus varies between 205 and 225 GPa and hence, the space was set to 190–240 GPa. Following Tabor's relationship of hardness and (JH) model results (Table 2), the yield stress at 0% plastic strain of steel can reach approximately 2400, 2600 and 2700 MPa, for substrate bias voltages of −200 V, −500 V and −700 V, respectively. Therefore, the respective constraints for the initial yield stress σ_y ($\varepsilon_p = 0$) were set to 2000–2700 MPa. Furthermore, the strain hardening exponent and Poisson's ratio of martensitic stainless steel have been studied extensively in the past and it is typically accepted to be constant mechanical properties of magnitude of 0.1 and 0.3 [51], respectively.

For the CrN coating, several studies have evaluated its Young's modulus through an analytical approach (Oliver-Pharr method) or by

finite element modeling and found values between 100 and 437 GPa (Table 3). Based on (JH) model results (Table 2), Young's modulus of the CrN coating varies between 67 and 205 GPa and hence, the bound constraints have been defined between 50 and 240 GPa. For the yield stress, we can find in the literature values, identified from a finite element inverse analysis, in the range of 2–12 GPa (Table 3). Hence, the bound constraints have been defined between 1 and 15 GPa. For the strain hardening exponent, the bound constraints have been defined between 0 and 0.5. Finally, Poisson's ratio has been studied extensively in the past and it is typically accepted to be a constant mechanical property of magnitude of 0.22 [41]. The initial guess parameters were set to start within the bound constraints. Hence, a total of 5 parameters will be optimized, three for the CrN coating (E, σ_y and n) and two for the steel substrate (E and σ_y).

The capability of the inverse analysis proposed in this study to fit three different experimental indentation (P-h) curves of Fig. 2 is evidenced in Fig. 6. By comparing the optimized values of (E) and (σ_y) for both the coating and the substrate with their initial values, we can conducted that the variation was generally less than 10% which improve the accuracy of the methodology adopted in this work. Convergence of all optimized parameters has been achieved rapidly in less than 50 iterations whatever the substrate bias voltage. After convergence has been reached, the inverse analysis approach proposed in this study proved to be a highly reliable method for predicting the key material properties to generate a full elastic-plastic stress-strain curve of a given coating as detailed below.

3.2.2. *Sensitivity analysis*

The sensitivity of the predicted (P-h) curves, with respect to an FE simulation using a set of reference material properties (E, σ_y, n) to the individual variation of up to ± 20 %in the values of these properties is conducted. The indentation depth ratio: (h/hmax-Op) (maximum optimized indentation depth to the calculated indentation depth), and the indentation load ratio: (P/Pmax-Op) (maximum optimized indentation load to the calculated indentation load) are used to study the effect of the variation of these properties on the predicted (P-h) curves. In this section, only the predicted (P-h) curve for the CrN coating obtained at a substrate bias voltage of −700 V is used for the sensitivity analysis and it will be considered as a reference for the other conditions.

3.2.2.1. Effect of CrN coating's properties. The sensitivity of the predicted (P-h) curves to the individual variation of up to± 20 %in the values of the CrN properties (E, σ_y, n) is presented in Fig. 7. As can be seen in Fig. 7(a), yield strength has a low influence on the shape of the loading part of the predicted (P-h) curve. The predicted indentation depth and indentation load seem to be unaffected by the individual variation of this parameter. The same trend is observed for Young's modulus (Fig. 7(b)) and the strain hardening exponent (Fig. 7(c)). Furthermore, the shape of the unloading curve appears to remain unaltered particulary with the individual variation of Young's modulus. As a matter of fact, the shape of the loading and the unloading curve is mainly influenced by the elastoplastic properties and Young's modulus, respectively [51]. These results confirm that the substrate will have the main effect in comparison to that of the CrN coating as can be seen in the following section.

3.2.2.2. Effect of steel substrate properties. Fig. 8 presents the sensitivity of the predicted (P-h) curves to the individual variation of up to± 20 %in the values of the steel properties (E, σ_y). As can be seen in Fig. 8(a), yield strength largely influences the indentation load and the indentation depth of the (P-h) curve. This dependency between the yield strength and the indentation load is related to the fact that to produce yielding and consequently plastic flow a larger load is required. Furthermore, the shape of the unloading curve appears to remain unchanged with respect tothe individual variation of the yield strength. Otherwise, the

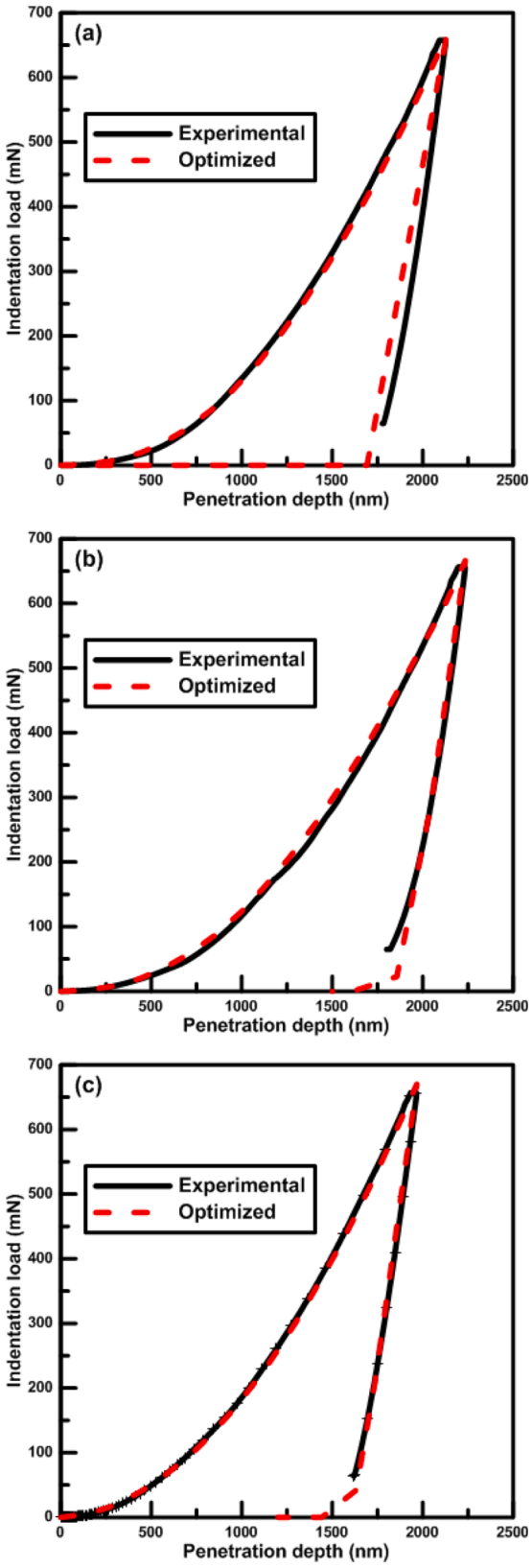

Fig. 6. Comparison of (P-h) curves obtained from experimental data and FE model using the optimized parameters for a substrate bias voltage of: (a) −200 V, (b) −500 V and (c) −700 V.

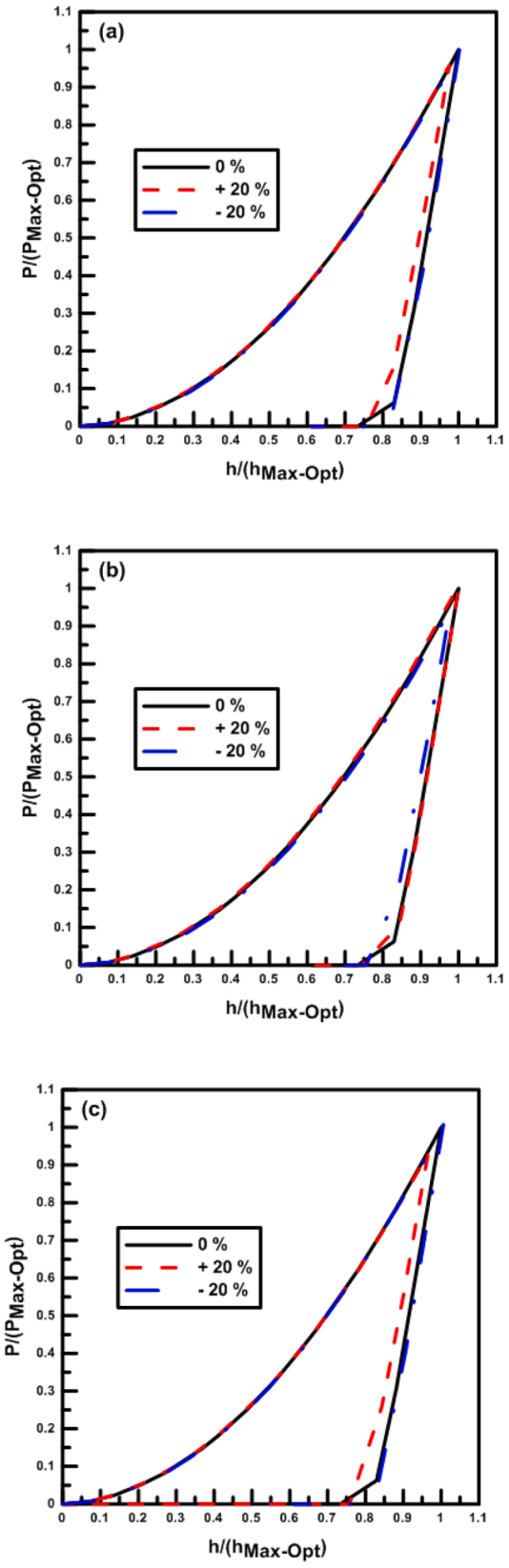

Fig. 7. Effects of the: (a) yield strength, (b)Young's modulus and (c) Strain hardening exponent of CrN coating on the predicted empirical parameters of loading and unloading.

individual variation of Young's modulus appears to modify not only the indentation load, and consequently the indentation depth, but also the unloading shape (Fig. 8(b)). This change is attributed to the contact stiffness (S) which depends on Young's modulus. These results confirm that the loading portion of the curve is mainly influenced by the yield strength whereas the unloading portion is more sensitive to Young's modulus. Furthermore, Fig. 8 shows that the substrate begins to interact and thus modifies the shape of the loading curve from a penetration depth of about 200 nm. This agrees with the results of the (JH) model (see Section 3.1).

As described above, from approximately 200 nm of penetration depth, the coating/substrate indentation responses are influenced by the substrate effects, which are reflected in the shape factors of (P-h) curves. It is noteworthy that only few differences can be detected from the (P-h) curves when varying the elastic-plastic properties of the CrN coating. Hence, the explicit values of (E), (σ_y), and (n) are not a critical issue in determining the indentation responses of the coating/substrate system. In the case of a hard film on a soft substrate, especially when the initial yield stress of both is very different, plastic deformation is restricted within the substrate while the film remains elastic. In addition, Young's modulus of the substrate is higher than that of the film, hence, the unloading curve will be more sensitive to Young's modulus of the substrate.

3.2.3. *Predicted elastic-plastic stress-strain curve of CrN coating*

Numerous experimental methods have been used to measure the elastic-plastic parameters of thin films, including the bulge [55] and micro-tensile [56]. However, both of these methods can only be carried out on freestanding films, requiring great efforts to strip the substrate from the film in whole or in part. Hence, difficulties in measuring the elastic-plastic properties of thin films by classical methods, through experimental stress-strain curve, have led to the use of the indentation method in nanoscale. The stress-strain curve of the thin film can be deducted from an optimization approach combined with a finite element modeling of the nanoindentation test.

The stress-strain elastic-plastic curve generated from nano-indentation finite element simulation for the CrN coatings performed with a substrate bias voltages of −200 V, −500 V and −700 V are shown in Fig. 9. It is obvious that CrN coating synthesized at a substrate bias voltage of −700 V exhibits the higher Young's modulus, Yield stress, and strain hardening exponent. These results confirm that the increase of the substrate bias voltage tends to enhance the mechanical properties of the film. In fact, when the substrate bias voltage increases, the structure of the CrN coating becomes denser and the vacant sites are reduced [36].

To verify the methodology, it was decided to compare the results of the optimization (Table 4) with the corresponding literature data for the CrN coating and the steel substrate (Table 3). For thin films, the measured material properties would depend on even more parameters as e.g. deposition technique, film quality, residual stresses between the substrate and thin film, film thickness, deposition conditions, methodology to extract the elasto-plastic properties, substrate effect, etc. Based on the literature data, it can be noticed that Young's modulus of the CrN coatings is comparable. Furthermore, the optimized values of the yield stress of the coating (Table 4) are higher than the estimated values through the Tabor assumption using the hardness values of coating given by the (JH) model (Table 2). These results indicate that H/3 is indeed inappropriate for CrN coating. The degree to which the yield stress here exceeds H/3 is consistent with the conical indentation FE results of Cheng and Li [57], as well as Dao et al. [58], taking into account obvious differences in the simulations (thick monolayer on a substrate versus bulk), in which the simulated hardness, (H), was equal to nearly twice H/3.

For the steel substrate, the mean value of Young's modulus calculated from the three optimiszd values in Table 4 is equal to 215 GPa which is coherent with the literature data (E between 190 GPa and 215 GPa). Moreover, the mean value of hardness of the steel substrate

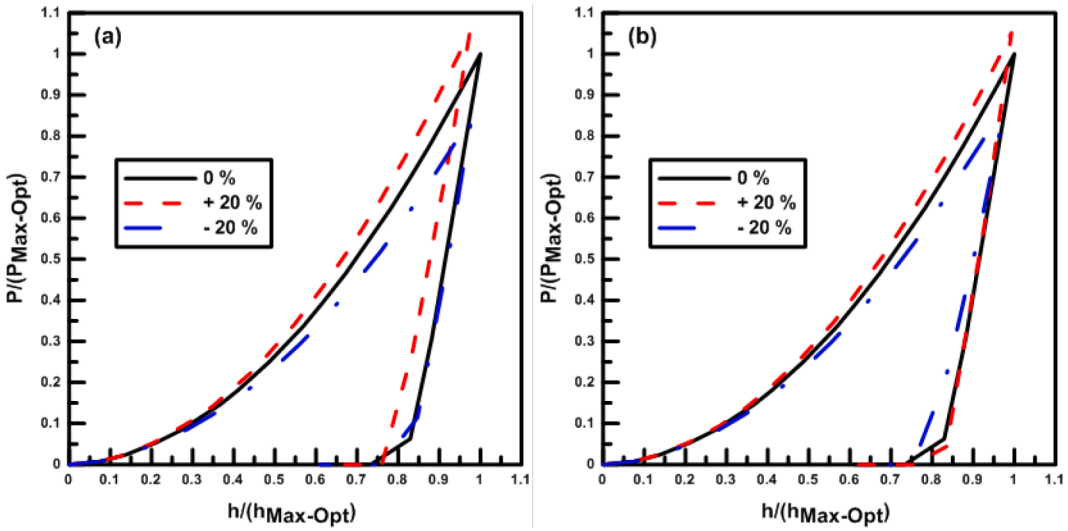

Fig. 8. Effects of the: (a) yield strength and (b) Young's modulus of the steel substrate on the predicted empirical parameters of loading and unloading.

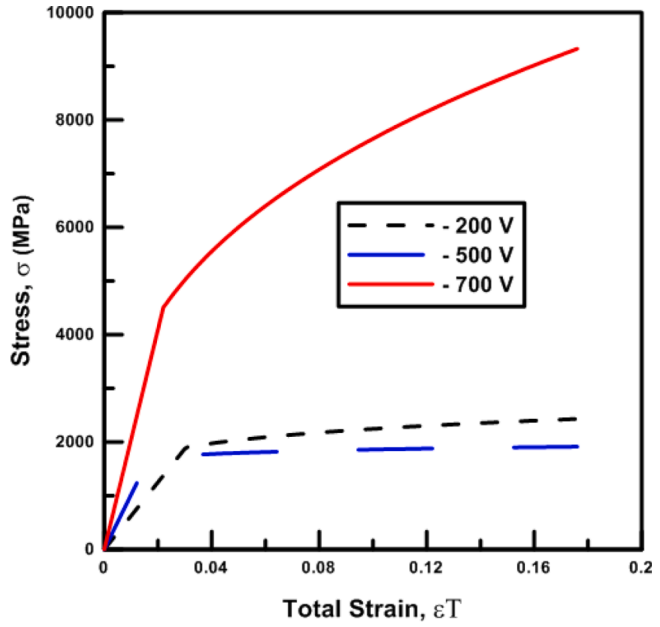

Fig. 9. Stress-strain curve built using the optimized CrN coating properties predicted by the inverse analysis as a function of the substrate bias voltage.

calculated from the values predicted by the (JH) model (see Table 2) is equal to 7.5 GPa which is coherent with the value reported in literature data ($H = 7$ GPa) [59]. Furthermore, the mean value of yield stress of the steel substrate calculated from the three optimized values in Table 4 is equal to 2.24 GPa, which is very close to the estimated values given through the Tabor assumption, H/3 ($\sigma_y = 7/3 = 2.3$ GPa).

4. Conclusions

In this work, a trust-region optimization algorithm is established to accurately predict a unique set of elastic-plastic properties of CrN coating (E, σ_y and n) through numerical and instrumental indentation when the indenter penetration depth is higher than the coating thickness. In the proposed methodology the accuracy of the predicted material properties from experimental load-displacement curves is addressed by narrowing the range of the initial values of the material properties based in the (JH) model and the literature data.

For the initial stage of the methodology, three CrN coated steel obtained with different substrate bias voltages were prepared and tested in nanoindentation. The (JH) model is used to estimate Young's modulus and the yield stress of the CrN coating and the substrate in order to integrate them subsequently into the reverse analysis as initial input parameters. Afterward, the elastic-plastic properties of the coating (E, σ_y and n) were obtained by fitting the numerical material response to the experimental data as well as by varying the elastic-plastic properties of the coating and the substrate. As a result, the stress-strains CrN coating characteristics were generated.

The sensitivity analyses were done in the numerical model by varying the preselected plasticity parameters of the CrN coating (E, σ_y and n) and of the substrate (E and σ_y). The results highlighted that the elasto-plastic parameters of the substrate (E and σ_y) has the most significant influence on both load-displacement in comparison with those of the CrN coating. The results showed a high impact on the loading curvature and consequently the value of a maximum depth (hmax) due to variations in (E) and (σ_y) of the steel substrate, respectively. Additionally, the sensitivity analyses provided evidence of the effect of Young's modulus on the value of contact stiffness (S) of the material during unloading, which controls the slope of the unloading section in a typical (P-h) curve.

The capability of the inverse analysis proposed in this study to predict a unique set of material properties that define the elastic-plastic stress-strain relationship of the coating is supported and validated by its capability of fitting the experimental (P-h) curves when the indentation depth is higher than the film thickness. This methodology can be applied in the case of multilayer coating system in which a high number of properties parameter must be optimized.

CRediT authorship contribution statement

Yamen Ben Ammar: Designed the model and the computational framework and analysed the data, wrote the paper with input from all authors.

Khalil Aouadi: Conceived and planned the experiments, contributed to the final version of the manuscript.

Corinne Nouveau: Supervised the project, contributed to the final version of the manuscript.

Aurélien Besnard: Aided in interpreting the experimental results.

Alex Montagne: Aided in interpreting the experimental results, verified the analytical methods, contributed to the final version of the manuscript.

All authors provided critical feedback and helped shape the research,

analysis and manuscript.

References

[1] X. Xing, Y. Wang, G. Xiao, X. Shu, S. Yu, Y. Wu, Identifying the elastoplastic properties of ductile film on hard substrate, Vacuum 189 (2021), 110252, https://doi.org/10.1016/j.vacuum.2021.110252.

[2] H. Abib, A. Iost, A. Montagne, K. Rahmoun, B. Ayachi, J. Vilcot, Investigations on the mechanical properties of the elementary thin films composing a $CuIn_{1-x}Ga_xSe_2$ solar cell using the nanoindentation technique, Thin Solid Films 633 (2017) 71–75, https://doi.org/10.1016/j.tsf.2016.11.013.

[3] A. Iost, G. Guillemot, Y. Rudermann, M. Bigerelle, A comparison of models for predicting the true hardness of thin films, Thin Solid Films 524 (2012) 229–237, https://doi.org/10.1016/j.tsf.2012.10.017.

[4] L. Li, L. Encarnacao, K. Brown, Polymer nanomechanics: separating the size effect from the substrate effect in nanoindentation, Appl. Phys. Lett. 110 (2017), 043105, https://doi.org/10.1063/1.4975057.

[5] J. Wang, X. Zheng, H. Zheng, Z. Zhu, S. Song, Evaluation of the substrate effect on indentation behavior of film/substrate system, Appl. Surf. Sci. 256 (2010) 5998–6002, https://doi.org/10.1016/j.apsusc.2010.03.108. OF THIN-FILM-SUBSTRATE SYSTEM: **OF FILM HARDNESS** ANDG'S MODULUS*.

[6] N. Tayebi, A. Polycarpou, T. Conry, Effects of substrate on determination of hardness of thin films by nanoscratch and nanoindentation techniques, J. Mater. Res. 19 (2004) 1791–1802, https://doi.org/10.1557/JMR.2004.0233.

[7] C. Gamonpilas, E. Busso, On the effect of substrate properties on the indentation behaviour of coated systems, Mater. Sci. Eng. A 380 (2004) 52–61, https://doi.org/10.1016/j.msea.2004.04.038.

[8] W.C. Oliver, G.M. Pharr, An improved technique for determining hardness and elastic modulus using load and displacement sensing indentation experiments, J. Mater. Res. 7 (6) (1992) 1564–1583, https://doi.org/10.1557/JMR.1992.1564.

[9] R. Saha, W.D. Nix, Effects of the substrate on the determination of thin film mechanical properties by nanoindentation, Acta Mater. 50 (1) (2002) 23–38, https://doi.org/10.1016/S1359-6454(01)00328-7.

[10] M. Doerner, W. Nix, A method for interpreting the data from depth-sensing indentation instruments, J. Mater. Res. 4 (1986) 601–609, https://doi.org/10.1557/JMR.1986.0601.

[11] Y. Jung, B. Lawn, M. Martyniuk, H. Huang, X. Hu, Evaluation of elastic modulus and hardness of thin films by nanoindentation, J. Mater. Res. 19 (2004) 3076–3080, https://doi.org/10.1557/JMR.2004.0380.

[12] X. Hu, B. Lawn, A simple indentation stress-strain relation for contacts with spheres on bilayer structures, Thin Solid Films 322 (1998) 225–232, https://doi.org/10.1016/S0040-6090(97)00919-X.

[13] H. Bückle, L'essai de micro dureté et ses applications, Publications scientifiques et techniques du ministère de l'air, NT90 Paris, 1960.

[14] B. Jönsson, S. Hogmark, Hardness measurements of thin films, Thin Solid Films 114 (1984) 257–269, https://doi.org/10.1016/0040-6090(84) 90123-8.

[15] E. Puchi-Cabrera, M. Staia, A. Iost, Modeling the composite hardness of multilayer coated systems, Thin Solid Films 578 (2015) 53–62, https://doi.org/10.1016/j.tsf.2015.01.070.

[15] A. Korsunsky, M. McGurk, S. Bull, T. Page, On the hardness of coated systems, Surf. Coat. Technol. 99 (1998) 171–183, https://doi.org/10.1016/S0257-8972(97)00522-7.

[17] K. Rahmoun, A. Iost, V. Keryvin, G. Guillemot, N. Chabane Sari, A multilayer model for describing hardness variations of aged porous silicon low-dielectric-constant thin films, Thin Solid Films 518 (2009) 213–221, https://doi.org/10.1016/j.tsf.2009.07.040.

[18] Z. Chen, X. Wang, A. Atkinson, N. Brandon, Spherical Indentation of Porous Ceramics: elasticity and Hardness, J. Eur. Ceram. Soc. 36 (2016) 1435–1445, https://doi.org/10.1016/j.jeurceramsoc.2015.12.049.

[19] M. Lichinchi, C. Lenardi, J. Haupt, R. Vitali, Simulation of Berkovich nanoindentation experiments on thin films using finite element method, Thin Solid Films 312 (1998) 240–248, https://doi.org/10.1016/S0040-6090(97)00739-6.

[20] H. Li, J. Chen, Q. Chen, M. Liu, Determining the constitutive behavior of nonlinear visco-elastic-plastic PMMA thin films using nanoindentation and finite element simulation, Mater. Des. 197 (2021), 109239, https://doi.org/10.1016/j.matdes.2020.109239.

[21] Y. Liao, Y. Zhou, Y. Huang, L. Jiang, Measuring elastic-plastic properties of thin films on elastic-plastic substrates by sharp indentation, Mech. Mater. 41 (2009) 308–318, https://doi.org/10.1016/j.mechmat.2008.10.008.

[22] L. Jiang, Y. Zhou, Y. Huang, Elastic-plastic properties of thin film on elastic-plastic substrates characterized by nanoindentation test, Trans. Nonferrous Met. Soc. China 20 (2010) 2345–2349, https://doi.org/10.1016/S1003-6326(10)60653-X.

[23] H. Zheng, X. Zheng, S. Song, J. Sun, F. Jiao, W. Liu, G. Wang, Evaluation of the elastic modulus of thin film considering the substrate effect and the geometry effect of indenter tip, Comput. Mater. Sci. 50 (2011) 3026–3031, https://doi.org/10.1016/j.commatsci.2011.05.022.

[24] M. Zhao, X. Chen, Y. Xiang, J. Vlassak, D. Lee, N. Ogasawara, N. Chiba, Y. Gan, Measuring elastoplastic properties of thin films on an elastic substrate using sharp indentation, Acta Mater. 55 (2007) 6260–6274, https://doi.org/10.1016/j.actamat.2007.07.045.

[25] N. Chakroun, A. Tekaya, H. Belhadjsalah, T. Benameur, A New Inverse Analysis Method for Identifying the Elastic Properties of Thin Films Considering Thickness and Substrate Effects Simultaneously, Int. J. Appl. Mech. 9 (2017), 1750096, https://doi.org/10.1142/S175882511750096X.

[26] W. Oliver, G. Pharr, Measurement of hardness and elastic modulus by instrumented indentation: advances in understanding and refinements to methodology, J. Mater. Res. 19 (2004) 3–20, https://doi.org/10.1557/jmr.2004.19.1.3.

[27] S. Kossman, A. Iost, D. Chicot, D. Mercier, I. Munoz, F. Roudet, P. Dufrenoy, V. Magnier, A. Cristol, Mechanical characterization by multiscale instrumented indentation of highly heterogeneous materials for braking applications, J. Mater. Sci. 54 (2019) 4647–4670, https://doi.org/10.1007/s10853-018-3158-7.

[28] J.J. Kang, A.A. B.ecker, W. Sun, Determining elastic-plastic properties from indentation data obtained from finite element simulations and experimental results, Int. J. Mech. Sci. 62 (2012) 34–46, https://doi.org/10.1016/j.ijmecsci.2012.05.011.

[29] T. Coleman, M.A. B.ranch, A. Grace, Optimization Toolbox for Use with MATLAB: user's Guide, Version 2, Math Works, Incorporated (1999).

[30] G. Papazafeiropoulos, M. Muñiz-Calvente, E. Martínez-Pañeda, Abaqus2Matlab: a suitable tool for finite element post-processing, Adv. Eng. Softw. 105 (2017) 9–16, https://doi.org/10.1016/j.advengsoft.2017.01.006.

[31] L. Liu, N. Ogasawara, N. Chiba, X. Chen, Can indentation technique measure unique elastoplasticproperties? J. Mater. Res. 24 (2009) 784–800, https://doi.org/10.1557/jmr.2009.0100.

[32] K. Tho, S. Swaddiwudhipong, Z. Liu, K. Zeng, J. Hua, Uniqueness of reverse analysis from conical indentation tests, J. Mater. Res. 19 (2004) 2498–2502, https://doi.org/10.1557/JMR.2004.0306.

[33] B. Arrazat, V. Mandrillon, K. Inal, Nanoindentation de couches dures ultra minces de ruthénium sur Or, Mater. Tech., (Les Ulis, Fr.) 99 (2011) 245–252, https://doi.org/10.1051/mattech/2011031 (In French).

[34] C. Shaohua, L. Lei, W. Tzuchiang, Nanoindentation of thin-film-substrate system: determination of film hardness and Young's modulus, Acta Mech. Sin. 20 (2004) 383–392, https://doi.org/10.1007/BF02489376.

[35] J. Romero, M. Gomez, J. Esteve, F. Montala, L. Carreras, M. Grifol, A. Lousa, CrAlN Coatings Deposited by Cathodic Arc Evaporation at Different Substrate Bias, Thin Solid Films 515 (2006) 113–117, https://doi.org/10.1016/j.tsf.2006.01.061.

[36] K. Aouadi, B. Tlili, C. Nouveau, A. Besnard, M. Chafra, R. Souli, Influence of Substrate Bias Voltage on Corrosion and Wear Behavior of Physical Vapor Deposition CrN Coatings, J. Mater. Eng. Perform. 28 (2019) 2881–2891, https://doi.org/10.1007/s11665-019-04033-y.

[37] Q. Ma, L. Li, Y. Xu, J. Gu, L. Wang, Y. Xu, Effect of Bias Voltage on TiAlSiN Nanocomposite Coatings Deposited by HiPIMS, Appl. Surf. Sci. 392 (2017) 826–833, https://doi.org/10.1016/j.apsusc.2016.09.028.

[38] Y. Lv, L. Ji, X. Liu, H. Li, H. Zhou, J. Chen, Influence of Substrate Bias Voltage on Structure and Properties of the CrAlN Films Deposited by Unbalanced Magnetron Sputtering, Appl. Surf. Sci. 258 (2012) 3864–3870, https://doi.org/10.1016/j.apsusc.2011.12.048.

[39] J. Ding, Q. Wang, Z. Liu, S. Jeong, T. Zhang, K. Kim, Influence of Bias Voltage on the Microstructure, Mechanical and Corrosion Properties of AlSiN Films Deposited by HiPIMS Technique, J. Alloys Compd. 772 (2019) 112–121, https://doi.org/10.1016/j.jallcom.2018.09.063.

[40] A. Munoz, E. Parra, F. Sequeda, CrN coatings deposited by magnetron sputtering: mechanical and tribological properties, Dyna (Medellin) 82 (2015) 147–155, https://doi.org/10.15446/dyna.v82n191.43292.

[41] T.B. Bobzin, R. Brugnara, M. Arghavani, T. Yang, Y. Chang, S. Chang, Investigation on plastic behavior of HPPMS CrN, AlN and CrN/AlN-multilayer coatings using finite element simulation and nanoindentation, Surf.Coat. Technol. 284 (2015) 310–317, https://doi.org/10.1016/j.surfcoat.2015.07.081.

[42] S. Tien, J. Duh, Effect of heat treatment on mechanical properties and microstructure of CrN/AlN multilayer coatings, Thin Solid Films 494 (2006) 173–178, https://doi.org/10.1016/j.tsf.2005.08.198.

[43] K. Malyska, M. Wojtan, K. Wasmer, K. Hejduk, J. Michler, In-situ SEM indentation studies of the deformation mechanisms in TiN, CrN and TiN/CrN, Micron 40 (2009) 22–27, https://doi.org/10.1016/j.micron.2008.02.013.

[44] A. Tekaya, H. Ghulman, T. Benameur, S. Labidi, Cyclic Nanoindentation and Finite Element Analysis of Ti/TiN and CrNNanocoatings on Zr-Based Metallic Glasses Mechanical Performance, J. Mater. Eng. Perform. 23 (2014) 4259, https://doi.org/10.1007/s11665-014-1212-4, 4270.

[45] E. Cameiro, N. Parreira, T. Vuchkov, A. Cavaleiro, J. Ferreira, M. Andritschky, S. Carvalho, Cr-Based Sputtered Decorative Coatings for Automotive Industry, Materials (Basel) 14 (2021) 5527, https://doi.org/10.3390/ma14195527.

[46] A. Jallad, A Study of the Plastic Deformation of CrN Coatings Deposited by RF Sputtering, in: M. Chouchane, T. Fakhfak, H. Daly, N. Aifaoui, F. Chaari (Eds.), Design and Modeling of Mechanical Systems - II. Lecture Notes in Mechanical Engineering, Springer, Cham, 2015, pp. 357–364, https://doi.org/10.1007/978-3-319-17527-0_36.

[47] Q. Li, L. Yang, Z. Wang, H. Zhang, Z. Liu, Q. Chen, The superior properties of CrN coatingsprepared by high power pulsed reactive magnetron sputtering, AIP Adv. 10 (2020), 015125, https://doi.org/10.1063/1.5132783.
[48] S. Tan, X. Zhang, X. Wu, F. Fang, Effect of Graded Bias on Microstructure and Hardness of CrN_X Films, Adv. Mater. Res. 154-155 (2010) 1476–1480, https://doi.org/10.4028/www.scientific.net/AMR.154-155.1476.
[49] M. Karimpour, D. Balinta, K. Malyska, A. Szerling, J. Michler, J. Lin, An inverse method for extracting the mechanical properties of the constituent materials of a multilayer from nanoindentation data, Comput. Mater. Sci. 68 (2013) 384–390, https://doi.org/10.1016/j.commatsci.2012.11.007.
[50] M. Vente, D. Arbelaez, J. Rocha, G. Rodriguez, A. Ovalle, J. Hernandez, J. Orozco, Effect of Graded Bias Voltage on the microstructure of arc-PVD CrN Films and its Response in Electrochemical & Mechanical Behavior, Appl. Phys. (2018) 1–14, https://doi.org/10.48550/arXiv.1810.07293.
[51] O. Iracheta, C. Bennett, W. Sun, Characterization of material property variation across an inertia friction welded CrMoV steel component using the inverse analysis of nanoindentation data, Int. J.Mech. Sci. 107 (2016) 253–263, https://doi.org/10.1016/j.ijmecsci.2016.01.023.
[52] D. Tabor, The hardness of metals. Oxford Classic Texts in the Physical Sciences, Oxford University Press, Oxford, 1951.
[53] Y. Tirupataiah, G. Sundararajan, On the constraint factor associated with the indentation of workhardening materials with a spherical ball, J. Mater.Transac.,A 22 (1991) 2375–2384, https://doi.org/10.1007/BF02665003.
[54] R. Sola, R. Giovanardi, G. Parigi, P. Veronesi, A Novel Methods for Fracture Toughness Evaluation of Tool Steels with Post-Tempering Cryogenic Treatment, Metals (Basel) 7 (2017) 75–84, https://doi.org/10.3390/met7030075.
[55] H. Javed, B. Merle, E. Preib, R. Hivet, A. Benedetto, M. Goken, Mechanical characterization of metallic thin films by bulge and scratch testing, Surf. Coating. Technol. 289 (2016) 69–74, https://doi.org/10.1016/j.surfcoat.2016.01.051.
[56] H. Huang, F. Spaepen, Tensile testing of free-standing Cu, Ag and Al thin films and Ag/Cu multilayers, Acta Mater. 48 (12) (2000) 3261–3269, https://doi.org/10.1016/S1359-6454(00)00128-2.
[57] Y. Cheng, Z. Li, Hardness obtained from conical indentations with various one angles, J. Mater. Res. 15 (2000) 2830–2835, https://doi.org/10.1557/JMR.2000.0404.
[58] M. Dao, N. Chollacoop, K. Vliet, T. Venkatesh, S. Suresh, Computational modeling of the forward and reverse problems in instrumented sharp indentation, Acta Mater. 49 (2001) 3899–3918, https://doi.org/10.1016/S1359-6454(01)00295-6.
[59] C. Nouveau, P. Steyer, K. Rao, D. Lagadrillere, Plasma nitriding of 90CrMoV8 tool steel for the enhancement of hardness andcorrosion resistance, Surf. Coating. Technol. 205 (2011) 4514–4520, https://doi.org/10.1016/j.surfcoat.2011.03.087.